$Ca_V1.2$ and $Ca_V1.3$ voltage-gated L-type Ca^{2+} channels in rat white fat adipocytes.

Authors: Olena A. Fedorenko*, Pawitra Pulbutr****, Elin Banke**, Nneoma E Akaniro-Ejim*, Donna C Bentley***, Charlotta S. Olofsson**, Sue Chan* and Paul A. Smith*

Affiliations: *School of Life Sciences, University of Nottingham, UK

**** Faculty of Pharmacy, Mahasarakham University, 44150 Thailand

*** School of Sport, Exercise and Health Sciences, Loughborough University, UK

** Department of Physiology/Metabolic Physiology, Institute of Neuroscience and Physiology, The Sahlgrenska Academy at University of Gothenburg Göteborg, Sweden.

Corresponding author: Dr PA Smith Address as above Paul.a.smith@nottingham.ac.uk

Short title Ca channels in white adipocytes

Key words: adipocyte, calcium channel, lipolysis, obesity

Word Count 4906 including abstract

Abstract

L-type channel antagonists are of therapeutic benefit in the treatment of hyperlipidaemia and insulin resistance. Our aim was to identify L-type voltage gated Ca^{2+} channels in white fat adipocytes, and determine if they affect intracellular Ca^{2+}, lipolysis and lipogenesis. We used a multidisciplinary approach of molecular biology, confocal microscopy, Ca^{2+} imaging and metabolic assays, to explore this problem using adipocytes isolated from adult rat epididymal fat pads. $Ca_V1.2$, $Ca_V1.3$ and $Ca_V1.1$ $alpha_1$, beta and $alpha_2$delta subunits were detected at the gene expression level. The $Ca_V1.2$ and $Ca_V1.3$ alpha1 subunits were identified in the plasma membrane at the protein level. Confocal microscopy with fluorescent antibodies labelled $Ca_V1.2$ in the plasma membrane. Ca^{2+} imaging revealed that the intracellular Ca^{2+} concentration, $[Ca^{2+}]_i$, was reversibly decreased by removal of extracellular Ca^{2+}, an effect mimicked by verapamil, nifedipine and Co^{2+}, all blockers of L-type channels. Whereas the Ca^{2+} channel agonist BAY-K8644 increased $[Ca^{2+}]_i$. The finding that the magnitude of these effects correlated with basal $[Ca^{2+}]_i$ suggests that adipocyte $[Ca^{2+}]_i$ is controlled by L-type Ca^{2+} channels that are constitutively active at the adipocyte depolarized membrane potential. Pharmacological manipulation of L-type channel activity modulated both basal and catecholamine-stimulated lipolysis but not insulin-induced glucose uptake or lipogenesis. We conclude that white adipocytes have constitutively active L-type Ca^{2+} channels which explains sensitivity of lipolysis to Ca^{2+} channel modulators. Our data suggest $Ca_V1.2$ as a potential novel therapeutic target in the treatment of obesity.

Introduction

White fat adipocytes (WFA) are the major energy depot of the body, storing and releasing energy in response to the calorific demands of the body during periods of excess and need respectively (Arner *et al.* 2011). It is widely accepted that an impairment of WFA triglyceride metabolism in obesity is a major etiological factor of the metabolic syndrome and type 2 diabetes. Whereby the inability of WFA to appropriately store energy as fat leads to ectopic disposition of lipids in insulin–responsive tissues such as skeletal muscle, liver and pancreas to promote insulin resistance and associated systemic disorders (Sattar & Gill 2014). To address dysfunctional fat storage, it is first necessary to understand the regulation of lipid storage in healthy WFA.

Extracellular Ca^{2+} influx is implicated in the processes of fat storage (Arruda & Hotamisligil 2015): lipolysis (Schimmel 1978; Izawa *et al.* 1983; Allen & Beck 2000) and lipogenesis (Avasthy *et al.* 1988). Indeed, studies in *Drosophila* mutants indicate that impaired adipocyte cytosolic Ca^{2+} is associated with increased lipid deposition (Baumbach *et al.* 2014). However, the identity of the Ca^{2+} pathway is unclear (Draznin *et al.* 1988).

Several routes by which Ca^{2+} enters primary WFA are identified, these include voltage-gated Ca^{2+} channels, VGCC (Clausen & Martin 1977; Pershadsingh *et al.* 1989) store-operated Ca^{2+} channels (El Hachmane & Olofsson 2018), and reverse mode Na^{+}/Ca^{2+} exchange, NCX (Pershadsingh *et al.* 1989; Bentley *et al.* 2014). Although VGCCs play a prominent role in Ca^{2+} entry and function of electrically excitable cells (Lipscombe 2004), this route of influx is ill-defined in non-excitable adipocytes.

Pharmacological investigations show that verapamil and nifedipine, blockers of L-type VGCCs, can inhibit WFA Ca^{2+} uptake (Martin *et al.* 1975; Pershadsingh *et al.* 1989) and impair glucose transport (Draznin *et al.* 1987), lipolysis (Izawa *et al.* 1983) and lipogenesis (Avasthy *et al.* 1988).

However, this inference of an association between Ca^{2+} influx and lipid turnover has come from independent studies where animal species, adipose depot as well as experimental conditions differed. To date, no comprehensive synthetic study exists where changes in Ca^{2+} influx and WFA function has been examined in primary adipocytes for the same species under similar experimental conditions of similar age and weight. Furthermore, a detailed molecular and immunohistochemical investigation of L-type VGCC expression in WFA is absent.

The aim of this study was to use a combination of Ca^{2+} imaging, metabolic, immunocytochemical and molecular biology techniques to identify L-type Ca^{2+} channels in WAT and demonstrate their functional role in lipid turnover.

Materials and Methods

Unless stated otherwise, adipocyte isolation and experiments were performed in Hank's buffer solution which composed of (in mM): NaCl 138, $NaHCO_3$ 4.2, KCl 5.6, $MgCl_2$ 1.2, $CaCl_2$ 2.6, NaH_2PO_4 1.2, glucose 5 and HEPES 10 (pH 7.4 with NaOH). For, nominally Ca^{2+} free solutions, $CaCl_2$ was equimolarly replaced with $MgCl_2$. All % values are weight per volume. Unless stated otherwise drugs and chemicals are from Sigma, Poole, UK

Ethical approval

Animal care and experimental procedures were carried out in accordance with either the UK Home Office Animals (Scientific Procedures) Act (1986) or Swedish ethical review board. In both instances the local ethical committees approved the animal procedures. Animals were killed by cervical dislocation or CO_2.

Isolation and preparation of adipocytes

Epididymal fat pads were taken from Wistar rats (fed *ad libitum,* 12 hr dark/light cycle, weight 220–420 g; Charles River Laboratory, Kent, UK). For some experiments tissue from Sprague Dawley rats were used, but since no difference could be detected, data was pooled. Adipocytes were isolated as described previously (Bentley *et al.* 2014).

PCR

For reverse transcriptase PCR (RT-PCR) total RNA was isolated by cell lysis in TRI Reagent. Genomic DNA was removed with RQ1 RNase-free DNase (Promega, UK) with RNA quantity and purity determined by the A_{260}/A_{280} ratio (1.98 to 2.02). The RNA integrity numbers (6-8) ascertained samples were suitable for RT-PCR (Schroeder *et al.* 2006). First-strand cDNA synthesis used 1 µg of total RNA with 200 ng random hexamer primers and Avian Myeloblastosis Virus reverse transcriptase (10 units/µl RNA, Promega).

PCR reactions used Dream Taq PCR Master Mix (ThermoFisher, UK) and primers shown in Table 1. PCR was performed at 95°C for 10 min, followed by 40 cycles at 95°C for 45 sec, 58°C for 45 sec, 72°C for 45 sec and terminated by a final extension step at 72°C for 10 min. PCR products were separated on 1% agarose gels, DNA stained with 0.5 µg/ml ethidium bromide and imaged with GeneSnap software (Syngene, UK). cDNA sequencing (DeepSeq, Nottingham, UK) checked PCR product identity.

Quantitative PCR (qPCR) reactions were performed in triplicate with SYBR® Green JumpStart TM Taq ReadyMix TM. The thermal profile was 10 minutes at 95°C, 40 cycles of denaturation at 95°C for 15 seconds, annealing for 20 seconds at the primer specific temperature, and elongation at 72°C for 35 seconds. The resultant mean threshold cycle (Ct) values were used for gene normalization and expression analyses. Three, stable, reference genes with the sequences listed in Table 2 were used: glyceraldehyde-3-phosphate dehydrogenase (GAPDH), phosphoglycerate kinase 1 (PGK1) and hypoxanthine guanine phosphoribosyl transferase (HPRT1)

(Gorzelniak *et al.* 2001; Fink *et al.* 2008; Silver *et al.* 2008). Relative mRNA levels were quantified by the method of Pfaffl (Pfaffl 2001).

Western blot analysis

Cytosolic and solubilized plasma membrane proteins were prepared by differential centrifugation. Cell lysates were prepared at 4°C with a lysis solution that contained 10 µl of protease inhibitor cocktail per 1 ml of lysis buffer (10 mM tris, 250 mM sucrose, 1 mM EDTA, pH 7.4). Protein content was determined by Lowry. 15-20 µg of protein was resolved by SDS-PAGE on 4-20% gradient precast minigels TGX (Biorad, UK) at 170 volts for 40 minutes.

Protein transfer onto nitrocellulose membranes was performed at 100 volts for 60 minutes in cold transfer buffer; Ponceau S staining confirmed transfer. Membranes were blocked in 5% milk in TBST (25mM Tris, pH 7.6; 125 mM NaCl; 0.1% Tween 20) for 3-4 hours, at 20-22°C, followed by overnight incubation at 4°C with primary antibodies: rabbit anti-$Ca_V1.3$ at 1:200 (ACC-005, Alomone), anti $Ca_V1.2$ at 1:500 dilution (ACC-003, Alomone), anti-β-actin at 1:5,000 and anti-Na,K-ATPase at 1:20,000 (Abcam, UK). Membranes were washed with TBST and incubated for 1 hour at room temperature with a 1:10,000 dilution of secondary antibodies: IRDye 800 CW goat anti-rabbit IgG (Li-COR™) and IRDye 680 CW goat anti-mouse IgG (Li-COR™). Antibody dilutions were made in 5% milk in TBST. Membranes were then washed with TBST, rinsed in H_2O and imaged with Li-COR Odyssey infrared Imaging System.

Band intensity was measured using the Li-COR Odyssey software version 2.1 (Li-COR Bioscience, USA) and analyzed using Image Studio Lite Version 5.2. For each protein band the signal intensity was normalized to that of β-actin expression, which was then expressed relative to that in brain. In initial experiments GAPDH was used as a control, but since comparison of the ratios obtained with that of β-actin expression showed no difference, the two set of data were pooled. For $Ca_V1.2$ in brain, bands spanning 130-250 kD were combined before normalization to β-actin. Samples probed

with the primary antibodies in the absence of primary antiserum indicated absence of non-specific binding

Immunocytochemistry

Adipocytes were attached to poly-L-lysine (25-100 µg ml-1) coated coverslips and fixed with 4% PFA for 10 min. Cells were permeablised in blocking buffer (PBS with 3% BSA and 0.5% Triton-100x) for 10 min then stained with primary anti-Calcium Channel L-type alpha 1C subunit (cacna1C) antibody conjugated with Atto 594 (ACC-003-AG, Alomone,) at 1:200 dilution for 16 hours (Raifman *et al.* 2017). To visualize nuclei cells were stained with Hoechst 33342 (8 µM for 30 min). Positive controls were initially performed with pancreatic beta-cell that express $Ca_V1.2$ (Schulla *et al.* 2003). Images were captured on a Zeiss LSM880C confocal microscope with excitation wavelengths of 405nm for Hoechst33342 and 633nm for the anti-CaV1.2-ATTO antibody.

Measurement of $[Ca^{2+}]_i$

Adipocytes attached to coverslips were incubated with the Ca^{2+} fluorophore Fluo-4 AM (1 µM; Molecular Probes) in Hank's solution with 0.01% BSA for 30 minutes at 21-23°C in the dark. Coverslips were mounted in a perifusion chamber on an Axiovert 135 Inverted microscope equipped for epifluorescence (Carl Zeiss Ltd, UK). Cells were focused to maximize equatorial circumference and fluorescence. Adipocytes were identified under Kohler illumination as 50-100 µm diameter spheroids with a nuclear protuberance (Fig. 3). Experiments were performed 1-4 hour post isolation.

Fluo-4 was excited at 450-490 nm, the emitted light band-pass filtered at 515-565 nm and the signal detected using a Photonics Science ISIS-3 camera with image intensification (luminous gain 8,000:1). Fluorescence emission was integrated for 900 ms and captured at 1Hz with an 8-bit frame grabber (DT3155, Data Translation, Basingstoke, UK) and Imaging Workbench Ver. 6.0 software (Indec Biosystems, Santa Clara, CA, USA).

Cells were perifused at 1 ml min^{-1}. Since dye extrusion occurred at temperatures >30°C, experiments were performed at 27-28°C.

For data analysis, a region of interest (ROI) was drawn around each cell, background corrected and the time course of its mean fluorescent intensity calculated. Fluorescence was calibrated by a two-point method (Ni *et al.* 1994): the maximum fluorescence value, Fmax; determined by permeabilization of the cells with Triton X-100 (0.0125-0.1%) followed by 10mM EGTA to determine the minimum, Fmin. $[Ca^{2+}]_i$ was calculated with the equation (Equation 1):

$$[Ca^{2+}]_i = Kd \times \frac{(F - F\min)}{(F\max - F)}$$

Where F is the background corrected fluorescence, and Kd the dissociation constant of Fluo-4: 345 nM (Bentley *et al.* 2014). Over 75% of basal $[Ca^{2+}]_i$ values measured were below the Kd of the dye and thus within its linear region of sensitivity. Data was only used from cells in which $[Ca^{2+}]_i$ was stable and had a basal value within the 5-95% percentile range (60-380 nM).

To visualize spatial variation of $[Ca^{2+}]_i$ it is necessary to mitigate fluorescent signal heterogeneity due to uneven dye loading or/and differences in cytoplasmic volume. In the absence of extracellular Ca^{2+}, Ca^{2+} influx is abolished and heterogeneity in fluorescence was assumed to reflect variation in only cell volume and dye loading. Since these parameters proportionally affect Fluo-4 fluorescence, a ratio of the fluorescence signal in the presence of extracellular Ca^{2+} with that in its absence was undertaken Using ImageJ2 with floating point arithmetic (Rueden *et al.* 2017) to normalize these confounders to reveal true differences in spatial $[Ca^{2+}]_i$.

Biochemical assays

To control for differences in adipocyte cell-density, biochemical data were normalized to paired values measured under basal or control conditions. Experiments were performed at 37°C.

Free fatty acid assay

Free fatty acid (FFA) release was used to measure lipolysis. Adipocytes were incubated for 60 minutes under different experimental conditions in 1 ml of Hank's. After which, 100 μl of supranatant was removed and stored at -20°C prior to assay. FFA was assayed with a non-esterified FFA assay kit (WAKO chemicals). After subtraction of blank, data was normalized to the absorbance of the FFA standard (17 μM oleic acid) and corrected for dilution.

Glucose uptake

Glucose-utilization was measured via ^{14}C glucose uptake. After a 30 minute pre-incubation under different experimental conditions, ^{14}C glucose was added and the cells incubated for a further 30 minutes, final volume 0.5 ml. For the assay, cells were separated from the medium by centrifugation and their ^{14}C content measured via scintillation counting. The GLUT-dependent glucose uptake was determined by subtraction of non-specific measured in the presence of 10 μM Cytochalasin B. For analysis, ^{14}C uptake was normalized to that measured in the absence of insulin and drug additions under control conditions.

Lipogenesis

Lipogenesis was measured via 3-^{3}H-glucose incorporation. Adipocytes were incubated for 30 minutes under different experimental conditions with a fixed activity of 3-^{3}H-glucose. For the assay, cells were separated from the medium by centrifugation and the ^{3}H content determined via scintillation counting. Lipogenesis was determined as the difference of cellular counts to that measured in the absence of 3-^{3}H-glucose. For analysis, lipogenesis

was normalized to that measured in the absence of insulin and drug additions under control conditions.

Justification of drug concentrations employed

Verapamil and nifedipine were used at concentrations employed by others to block L-type VGCCs in this cell type (Martin *et al.* 1975; Begum *et al.* 1992; Ni *et al.* 1994). Moreover, concentrations were employed to mitigate their adsorption by serum (>90%) (Rumiantsev *et al.* 1989) and absorption by the adipocytes (Louis *et al.* 2014).

Statistical analysis

Data were checked with the D'Agostino & Pearson omnibus normality test with the appropriate inferential test given in the text. Graphical data are shown as box and whisker plots as median, interquartile range, 10, and 90% confidence intervals. Unless otherwise stated, experiments were performed as repeated measures. Numerical data are quoted as means ± S.E.M. or median with 5 to 95% confidence intervals (95% C.I.), where n is the number of determinations. Experimental data was collated from at least four animals. Fitting of equations to data used a least squares algorithm with the parameters given in text. Statistical analysis was performed using Graphpad PRISM version 8.2 (San Diego, California USA). Data were considered statistically significant difference when $p < 0.05$ and in graphics is flagged as *, ** when $P < 0.01$, *** when $P < 0.001$ and **** when $P < 0.0001$.

Results

Molecular Evidence and identification of VGCC in WAT

RT-PCR indicated the presence of mRNA for $Ca_V1.1$, $Ca_V1.2$ and $Ca_V1.3$ but not $Ca_V1.4$ L-type $alpha_1$ subunits in epididymal WFA (Fig. 1A); mRNA for L-type VGCCs $beta_2$ subunits: *cacnb2, cacnb3* and *cacnb4,* and $alpha_2$delta subunits, *cacna2d1, cacna2d2 and cacna2d3* were also detected. cDNA sequence analysis of the PCR products for $Ca_V1.1$, $Ca_V1.2$ and $Ca_V1.3$ gave 98.7±0.3 (n=3), 98.5±0.2% (n=6) and 97.8±0.7% (n=6) identity to the rat VGCC subunits alpha1S (*Cacna1s*), alpha1C (*Cacna1c*) and alpha1D (*Cacna1d*) respectively. Quantification of mRNA levels by qPCR gave a rank expression order of $Ca_V1.2$ > $Ca_V1.3$ > $Ca_V1.1$ (Fig. 1B).

Western blots of the plasma membrane fraction revealed a 260 kD $Ca_V1.3$ alpha-subunit (Fig. 2B) (N'Gouemo *et al.* 2015) and an extended form of $Ca_V1.2$ of>250 kD (Fig. 2A); the latter bigger than the canonical neuronal isoform of 210 kD (Raifman *et al.* 2017). $Ca_V1.2$ protein expression was 10 fold greater than that of $Ca_V1.3$ (Fig. 2C; $p<0.001$, Mann Whitney); a ratio comparable the qPCR results (Fig. 1B)

Immunohistochemical evidence of VGCC in WAT

Confocal microscopy revealed that fixed adipocytes preserved their morphology (Fig. 3A) as demonstrated by retention of their nucleus and spherical form. Atto 594 labeled antibodies identified $Ca_V1.2$ in the plasma membrane; this was granular in appearance and densest near the nucleus (Fig. 3B). Given this finding, the spatial distribution of $[Ca^{2+}]_i$ was examined (Fig. 3C). Figure 3C shows six adipocytes with identifiable nuclei, all of which responded with a reversible decrease in $[Ca^{2+}]_i$ on removal of bath Ca^{2+} (Fig. 5A). Although the change in $[Ca^{2+}]_i$ was uniformly distributed in the extra-nuclear cell membrane for all six cells, three had a higher $[Ca^{2+}]_i$ in the perinuclear region (Fig. 3D); data which supports a higher density of VGCCs in this region.

Evidence for constitutive Ca^{2+} influx

Epifluorescent imaging of adherent adipocytes revealed a skewed basal $[Ca^{2+}]_i$ and Gaussian cell diameter distributions with median values of 135 nM (129 to 145 nM, 95% C.I., n = 555) and 80 μm (79 to 81 μm, 95% C.I., n = 580) respectively (Fig. 4A, B). $[Ca^{2+}]_i$ values are similar to those previously reported (Schwartz *et al.* 1991; Hardy *et al.* 1992; Ni *et al.* 1994; Gaur *et al.* 1998).

Both basal $[Ca^{2+}]_i$ (Spearman r = 0.17, 0.084 to 0.25 95% C.I., $p < 0.0001$, Fig. 4C) and body weight (Spearman r = 0.13, 0.01 to 0.26 95% C.I., $p < 0.05$, Fig. 4D) were positively correlated with adipocyte diameter, although $[Ca^{2+}]_i$ did not correlate with individual animal weight (Spearman, Fig. 4E).

To explore Ca^{2+} influx, the effect of equimolar substitution of extracellular Ca^{2+} with Mg^{2+} was investigated. Removal of bath Ca^{2+} reversibly decreased $[Ca^{2+}]_i$, $\Delta[Ca^{2+}]_i$, by 30% (25 to 34%, 95% C.I ; $p<0.0001$, Friedman; Figs. 5A, B). $\Delta[Ca^{2+}]_i$ was negatively correlated with basal $[Ca^{2+}]_i$: that is cells with the highest basal values underwent the largest percentage decrease on Ca^{2+} removal (Spearman r = -0.32, $P<0.001$; Fig. 5C). $\Delta[Ca^{2+}]_i$, was unrelated to cell diameter or body weight (Spearman). Prolonged exposure to Ca^{2+} removal for over three hours did not affect cell integrity which suggest that this intervention is not cytotoxic.

Doubling the extracellular Ca^{2+} concentration produced a 9% increase in $[Ca^{2+}]_i$ (4 to 16%, 95% C.I; $p<0.0001$ Wilcoxon Signed Rank; Figs. 5D, E). Conversely, addition of 2.5 mM Co^{2+}, an inorganic inhibitor of VGCCs, irreversibly decreased $[Ca^{2+}]_i$ by 13% (8 to 17%, 95% C.I; $p<0.0001$ Wilcoxon Signed Rank; Fig. 5D); a magnitude comparable to that seen with removal of extracellular Ca^{2+} (Fig. 5E).

Pharmacological manipulation of Ca^{2+} influx

We next tested a variety of pharmacological agents that affect VGCC activity. Although both verapamil and nifedipine significantly decreased $[Ca^{2+}]_i$ relative to DMSO control (Fig. 6) ($p<0.001$ and $p<0.0001$ respectively, Wilcoxon Signed Rank), the effect of nifedipine was small (Figs. 6B, F). Verapamil decreased $\Delta[Ca^{2+}]_i$ to a similar extent to Ca^{2+} removal (Kruskal Wallis, Fig. 6F). In the presence of nifedipine Ca^{2+} removal further decreased $[Ca^{2+}]_i$ (Figs. 6B, G). In any given cell, the amount by which verapamil decreased $[Ca^{2+}]_i$ positively correlated with that seen with extracellular Ca^{2+} removal (Pearson r = 0.77, slope 0.66 ± 0.13, $p<0.001$; Fig. 6H).

We next explored the pharmacology of $[Ca^{2+}]_i$ recovery following re-addition of Ca^{2+} to the bath after its removal. Both verapamil (Figs. 7B, F, J) and nifedipine (Figs. 7C, G, J) significantly affected $[Ca^{2+}]_i$ recovery (Figs. 7A, E, J); did. The NCX inhibitor SN-6 neither affected basal $[Ca^{2+}]_i$ or its recovery (Figs. 7H, J). BAY-K8644, an agonist of L-type VGCCs, significantly enhanced recovery (Figs. 7D, I, J).

L-type Ca^{2+} influx stimulates basal lipolysis

Since Ca^{2+} modulates the lipolytic cascade in WFA (Schimmel 1978; Izawa *et al.* 1983; Allen & Beck 2000), we investigated if L-type VGCCs affected lipolysis (Fig. 9). Isoprenaline stimulated lipolysis with a pEC_{50} of 7 (6.7 to 7.3, 95% C.I) and Hill coefficient of 0.8 (0.43 to 1.2, 95% C.I; Fig. 9A). At 10 μM, isoprenaline stimulated lipolysis 9.8 ± 0.63 fold ($p<0.001$, One Sample t test; n = 39). Consistent with previous reports (Izawa *et al.* 1983; Allen & Beck 2000), removal of extracellular Ca^{2+} neither affected the EC_{50} or Hill coefficient for isoprenaline, but decreased lipolysis by ~30% ($p<0.0004$; Figs. 8A, C). Insulin inhibited the beta-adrenoceptor stimulated lipolysis with a pEC_{50} of 9.4 (9.6 to 9.3, 95% C.I; Fig. 9B).

Interventions that promoted Ca^{2+} influx: BAY-K8644 or elevation of $[K^+]_o$ (Bentley *et al.* 2014), stimulated basal, but not isoprenaline-stimulated,

lipolysis (Figs. 8C, D). Interventions that decreased Ca^{2+} influx: removal of extracellular Ca^{2+} or verapamil inhibited both isoprenaline-stimulated and basal lipolysis (Fig. 8C, D). Insulin stimulated basal lipolysis (Fig. 8D), an effect consistent with its ability to elevate $[Ca^{2+}]_i$ (Clausen & Martin 1977). The capacity of 20 nM insulin to block beta-adrenoceptor stimulated lipolysis was unaffected by interventions that affected $[Ca^{2+}]_i$ (Fig. 8E).

We checked if intracellular Ca^{2+} handling affected lipolysis. 1 μM oxytocin, which mobilizes intracellular Ca^{2+} (Kelly *et al.* 1989), did not affect basal lipolysis (Fig. 8G), but consistent with others (Fain *et al.* 1997) inhibited isoprenaline-stimulated lipolysis (Fig. 8F). Neither store depletion with 1 μM thapsigargin (El Hachmane *et al.* 2018), or increased cytosolic Ca^{2+} buffering with 10 μM BAPTA-AM (Komai et al. 2014)affected isoprenaline-stimulated lipolysis Fig. 8F); however, both treatments impaired basal lipolysis (Fig. 8G); actions consistent with the greater sensitivity of basal lipolysis to $[Ca^{2+}]_i$ compared to that stimulated by isoprenaline (Figs. 8C, D).

Although alpha-adrenoceptor activation mobilizes intracellular Ca^{2+} stores in WFA (Hardy *et al.* 1992), like others (Blackmore, PF;Augert 1989; Seydoux *et al.* 1996), we did not see an increase in $[Ca^{2+}]_I$ with beta-adrenoceptor activation (n = 7).

L-type Ca^{2+} influx does not affect glucose uptake or lipogenesis

Insulin at 2 nM maximally stimulated glucose uptake 5 fold ($p<0.001$, One Sample t test) (Fig. 9A). Insulin–stimulated glucose uptake was unaffected by either 5 μM nifedipine or 1 μM BAY-K8644 (Figs. 9A, B); outcomes that were independent of insulin concentration. Lipogenesis was also maximally stimulated by 2 nM insulin (~9 fold, $p<0.001$, One Sample t test) (Figs. 10C, D). However, neither 5 μM nifedipine or 1 μM BAY-K8644 significantly affected lipogenesis (Figs. 10C, D).

427

Discussion

Molecular evidence for L-type Ca^{2+} channels

Our Western blot, PCR and in-situ immunolabelling data demonstrates expression of $Ca_V1.2$ and $Ca_V1.3$ L-type VGCCs in primary white fat adipocytes. The presence of $Ca_V1.2$/$Ca_V1.3$ in WFA is consistent with transcriptomic data published for human (Fagerberg *et al.* 2014) and mouse fat tissue (Yue *et al.* 2014); however, in contrast to these, we failed to detect $Ca_V1.4$. Although the 250 kD $Ca_V1.2$ protein band went undetected in our brain tissue control we did detect its 210 KD proteolytic cleavage product (Hell *et al.* 2017; Shi *et al.* 2017). Using the same antibody, others have also detected just a 210 kD $Ca_V1.2$ band (N'Gouemo *et al.* 2015). The 140 kD band may relate to the 130 kD or 150 kD non-Cav1.2 epitope that this antibody recognized in $Ca_V1.2$ knock out mice (Bavley *et al.* 2017; Hell *et al.* 2017). Though adipocytes possessed a $Ca_V1.2$ immuno-positive band, they did not show any further proteolytic cleavage products, data that suggests that this protein has post-translational modification with a polymorphic proteolytic cleavage site. For $Ca_V1.3$, we only obtained positive immunoblots with early batches of antibody, a recognized problem with commercial antibodies to $Ca_V1.3$ (Hell *et al.* 2017). In WFA, $Ca_V1.3$ was comparable in molecular weight to that observed in our brain controls and heart (268kD) (Le Scouarnec *et al.* 2008). The presence of mRNA for L-type VGCC $alpha_1$, $beta_2$ and $alpha_2$delta subunits suggests that adipocytes have the capacity to traffic and assemble functional VGCCs (Dolphin 2016).

Constitutive Ca^{2+} influx through L-type Ca^{2+} channels.

Our finding that both Co^{2+} and verapamil decreased $[Ca^{2+}]_i$ by similar amounts to Ca^{2+} removal is indicative of a Ca^{2+}-influx pathway mediated by L-type VGCCs. This notion is reinforced by enhancement of Ca^{2+} influx by the L-type VGCCs dihydropyridine agonist BAY-K8644. Our data contrasts to studies where neither nitrendipine or verapamil affected $[Ca^{2+}]_i$ under basal conditions (Gaur *et al.* 1996a, b). One possible reason for this

discrepancy is that we corrected for the effect of DMSO on fluorescence to reveal a block whereas previous studies had not.

The fact that removal of bath Ca^{2+} had a larger effect in adipocytes with higher basal $[Ca^{2+}]_i$ suggests that basal $[Ca^{2+}]_i$ is set by the prevalent VGCC activity. These findings, combined with the ability of verapamil and nifedipine to prevent, and BAY-K8644 to enhance Ca^{2+} recovery, suggest that basal $[Ca^{2+}]_i$ in WFA is maintained by a constitutive Ca^{2+} influx via L-type VGCCs; an idea supported by impairment of $^{45}Ca^{2+}$ uptake in WFA by L-type VGCCs antagonists (Martin *et al.* 1975).

The resting membrane potential of primary white adipocytes, measured by ourselves (Bentley *et al.* 2014) and others (Ramírez-Ponce *et al.* 1990; Lee & Pappone 1997), is around -30 mV. As this voltage is within the activation range of L-type VGCCs (Xu & Lipscombe 2001) a "window Ca^{2+} current" (Fleischmann *et al.* 1994) is expected. Constitutive L-type VGCC activity in electrically non-excitable cells is not unique; for example it has been recorded at a similar Vm (-30 mV) in osteoclasts (Miyauchi *et al.* 1990). To be constitutively active, inactivation of these VGCCs must be incomplete.

Although whole-cell voltage-clamp would have been ideal for electrophysiological characterization of the VGCCs we did not attempt this for technical reasons. First, the adipocyte cytoplasm is a relatively thin ~0.3 µm layer wrapped around a lipid droplet of ~80 µm diameter (Bentley *et al.* 2014); this creates a membrane time constant of 100's of ms (Bentley *et al.* 2014), compared to ~2 ms for a neuron (Coombs *et al.* 1956) of similar diameter (Henneman & Mendell 2010). This difference precludes voltage-clamping of VGCCs under physiological conditions due to space clamp considerations and "voltage escape" (Armstrong & Gilly 1992). Secondly, although Ca^{2+} influx can affect $[Ca^{2+}]_i$, we have previously shown that it is too small to affect Vm (Bentley *et al.* 2014), a result indicative of low channel density. Indeed, $^{45}Ca^{2+}$ tracer studies (Martin *et al.* 1975) have measured the DHP-sensitive Ca^{2+} influx in WFA at ~0.024 pmoles s^{-1} cm^{-2}:

~1.5 amoles s^{-1} $cell^{-1}$ or ~ 0.3 pA of whole-cell inward Ca^{2+} current, a value too low to measure with whole-cell voltage-clamp.

Constitutive Ca^{2+} influx modulates lipid metabolism

Our data confirms that both basal and stimulated lipolysis require extracellular Ca^{2+} (Bleicher *et al.* 1966; Ziegler *et al.* 1980; Allen & Beck 2000). However, we now show that lipolysis is sensitive to agents that modulate L-type VGCC activity. Although, isoprenaline-stimulated lipolysis could not be enhanced by interventions that increase $[Ca^{2+}]_i$, presumably because it was already maximal, like basal lipolysis, it was impaired by verapamil and Ca^{2+} removal. The idea that Ca^{2+}-influx promotes lipolysis is also supported by the action of high K^+, where substitution of bath Na^+ with K^+ elevates $[Ca^{2+}]_i$ by reverse Na^+-Ca^{2+} exchange (Bentley *et al.* 2014).

Multiple targets exist for extracellular Ca^{2+} during beta-adrenoceptor stimulated lipolysis. Extracellular Ca^{2+} enhances beta-adrenoceptor stimulated cAMP production (Ziegler *et al.* 1980) and is also required for undefined lipolytic processes downstream of cytosolic cAMP (Allen & Beck 2000). Indeed, lipolysis can be potentiated by increasing $[Ca^{2+}]_i$ with Ca^{2+} ionophores in the absence of cAMP elevation (Gaion & Krishna 1982) or conversely, as shown here, depressed with Ca^{2+} chelators (Efendić *et al.* 1970). However, the exact mechanisms by which Ca^{2+}, and indeed Ca^{2+} influx modulates basal lipolysis remains unknown; it is unlikely to involve the Ca^{2+}-sensitive, isoform III, of adenylyl cyclase found in WFA (Wang *et al.* 2009) since changes in Ca^{2+} influx do not affect adipocyte cAMP levels under basal conditions (Ziegler *et al.* 1980). However, adipocyte lipoprotein lipase is positively modulated by Ca^{2+} (Efendić *et al.* 1970; Soma *et al.* 1989; Carmen & Víctor 2006).

Translational context

The idea that Ca^{2+} influx via $Ca_V1.2/Ca_V1.3$ regulates basal lipolysis agrees with translational data. Rats with chronic renal failure are hyperlipidaemic and possess WFA with elevated intracellular Ca^{2+} levels (Ni *et al.* 1995). The observation that verapamil reversed these phenomena suggests that exacerbated Ca^{2}-influx via L-type VGCCs may be responsible for the elevated basal lipolysis. This notion is also supported by the ability of nicardipine to decrease plasma levels of FFA in spontaneously hypertensive rats (Cignarella 1994). Moreover, in humans, verapamil can also decrease basal plasma FFA levels, again data suggestive of VGCC mediated Ca^{2}-influx dependent lipolysis (Hvarfner *et al.* 1988). Such effects do not arise through impairment of beta-adrenoceptor activation since antihypertensives such as nicardipine and verapamil actually promote catecholamine levels through activation of baroreflex mediated sympathetic output. The failure of the DHP L-type channel antagonists to affect plasma FFA in man can be reconciled by the binding of these drugs to Cav1.2/1.3 being compromised by FFA (Pepe *et al.* 2006).

Conclusion

Our study provides direct, corroborative, evidence for the existence of $Ca_V1.2/Ca_V1.3$ L-type voltage-gated Ca^{2+} channels in white adipocytes. The basal concentration of intracellular Ca^{2+} appears to reflect the ambient level of VGCC activity on an individual cell basis, apparently unrelated to adipocyte size or animal weight. Importantly, $Ca_V1.x$ channels contribute to a persistent state of Ca^{2+} influx in WFA, without the need for cell excitability, and appear to have a key role in lipolysis. Consequently, dysregulation of $Ca_V1.x$ in WFA may contribute to lipid storage disorders that may contribute to, or indeed precipitate, the metabolic syndrome. As such, these cation channels may be a potential therapeutic target for the treatment of hyperlipidaemia, peripheral insulin resistance and obesity.

Declaration of interest, funding and acknowledgements

All of the authors declare that there is no conflict of interest that could be perceived as prejudicing the impartiality of the research reported. PP was in receipt of the Royal Thai Government scholarship. DCB was in receipt of a BBSRC studentship. NA is in receipt of a Schlumberger Foundation PhD fellowship. This work was supported by Diabetes UK (Grant ID: RB03CJ) , Leverhulme Trust (Grant ID: RPG-2017-162), Swedish Diabetes Foundation (DIA2015-062) and Swedish Medical Research Council (Grant ID: 2013-7107).

References

Allen D & Beck RRR 2000 Role of calcium ion in hormone-stimulated lipolysis. *Biochemical Pharmacology* **35** 767–772. (doi:10.1016/0006-2952(86)90244-3)

Armstrong CM & Gilly WF 1992 Access resistance and space clamp problems associated with whole-cell patch clamping. *Methods in Enzymology* **207** 100–122. (doi:10.1016/0076-6879(92)07007-B)

Arner P, Bernard S, Salehpour M, Possnert G, Liebl J, Steier P, Buchholz BA, Eriksson M, Arner E, Hauner H *et al.* 2011 Dynamics of human adipose lipid turnover in health and metabolic disease. *Nature* **478** 110–113. (doi:10.1038/nature10426)

Arruda AP & Hotamisligil GS 2015 Calcium Homeostasis and Organelle Function in the Pathogenesis of Obesity and Diabetes. *Cell Metabolism* **22** 381–397. (doi:10.1016/J.CMET.2015.06.010)

Avasthy N, Jeremy JY & Dandona P 1988 The role of calcium in mediating phorbol ester- and insulin-stimulated adipocyte lipogenesis. *Diabetes Research (Edinburgh, Scotland)* **9** 91–95.

Baumbach J, Hummel P, Bickmeyer I, Kowalczyk KM, Frank M, Knorr K, Hildebrandt A, Riedel D, Jäckle H & Kühnlein RP 2014 A Drosophila In Vivo Screen Identifies Store-Operated Calcium Entry as a Key Regulator of Adiposity. *Cell Metabolism* **19** 331–343. (doi:10.1016/j.cmet.2013.12.004)

Bavley CC, Fischer DK, Rizzo BK & Rajadhyaksha AM 2017 Cav1.2 channels mediate persistent chronic stress-induced behavioral deficits that are associated with prefrontal cortex activation of the p25/Cdk5-glucocorticoid receptor pathway. *Neurobiology of Stress* **7** 27–37. (doi:10.1016/J.YNSTR.2017.02.004)

Begum N, Sussman KE & Draznin B 1992 Calcium-induced inhibition of phosphoserine phosphatase in insulin target cells is mediated by the phosphorylation and activation of inhibitor 1. *Journal of Biological Chemistry* **267** 5959–5963.

Bentley DC, Pulbutr P, Chan S & Smith PA 2014 Etiology of the membrane

potential of rat white fat adipocytes. *American Journal of Physiology - Endocrinology and Metabolism* **307** E161–E175. (doi:10.1152/ajpendo.00446.2013)

Blackmore, PF;Augert G 1989 Effect of hormones on cytosolic free calcium in adipocytes. *Cell Calcium* **10** 561–567. (doi:10.1016/0143-4160(89)90018-3)

Bleicher BSJ, Farber L, Lewis A & Goldner MG 1966 Electrolyte-Activated Lipolysis In Vitro : Modifying Effect of Calcium. *Metabolism* **15** 742–748.

Carmen GY & Víctor SM 2006 Signalling mechanisms regulating lipolysis. *Cellular Signalling* **18** 401–408. (doi:10.1016/j.cellsig.2005.08.009)

Cignarella A 1994 Antithrombotic activity of nicardipine in spontaneously hypertensive rats. *Pharmacological Research* **30** 273–280. (doi:10.1016/1043-6618(94)80109-6)

Clausen BT & Martin BR 1977 The Effect of Insulin on the Washout .of 45Ca Calcium from Adipocytes and Soleus Muscle of the Rat. *Biochemical Journal* **164** 251–255.

Coombs JS, Curtis DR & Eccles JC 1956 Time Courses of Motoneuronal Responses. *Nature* **178** 1168–1169. (doi:10.1038/1781168a0)

Dolphin AC 2016 Voltage-gated calcium channels and their auxiliary subunits: physiology and pathophysiology and pharmacology. *Journal of Physiology* **594** 5369–5390. (doi:10.1113/JP272262)

Draznin B, Sussman K, Kao M, Lewis D & Sherman N 1987 The existence of an optimal range of cytosolic free calcium for insulin-stimulated glucose transport in rat adipocytes. *J Biol.Chem.* **262** 14385–14388.

Draznin B, Sussman KE, Eckel RH, Kao M, Yost T & Sherman NA 1988 Possible role of cytosolic free calcium concentrations in mediating insulin resistance of obesity and hyperinsulinemia. *The Journal of Clinical Investigation* **82** 1848–1852. (doi:10.1172/JCI113801)

Efendić S, Alm B & Löw H 1970 Effects of Ca^{++} on Lipolysis in Human Omental Adipose Tissue In Vitro. *Hormone and Metabolic Research* **2** 287–291. (doi:10.1055/s-0028-1095061)

628 Fagerberg L, Hallström BM, Oksvold P, Kampf C, Djureinovic D, Odeberg
629 J, Habuka M, Tahmasebpoor S, Danielsson A, Edlund K *et al.* 2014
630 Analysis of the human tissue-specific expression by genome-wide
631 integration of transcriptomics and antibody-based proteomics.
632 *Molecular & Cellular Proteomics : MCP* **13** 397–406.
633 (doi:10.1074/mcp.M113.035600)
634 Fain JN, Gokmen-Polar Y & Bahouth SW 1997 Wortmannin converts
635 insulin but not oxytocin from an antilipolytic to a lipolytic agent in the
636 presence of forskolin. *Metabolism: Clinical and Experimental*.
637 (doi:10.1016/S0026-0495(97)90169-4)
638 Fink T, Lund P, Pilgaard L, Rasmussen JG, Duroux M & Zachar V 2008
639 Instability of standard PCR reference genes in adipose-derived stem
640 cells during propagation, differentiation and hypoxic exposure. *BMC*
641 *Molecular Biology* **9** 1–9. (doi:10.1186/1471-2199-9-98)
642 Fleischmann BK, Murray RK & Kotlikoff MI 1994 Voltage window for
643 sustained elevation of cytosolic calcium in smooth muscle cells.
644 *Proceedings of the National Academy of Sciences of the United States*
645 *of America* **91** 11914–11918. (doi:10.1073/pnas.91.25.11914)
646 Gaion R & Krishna G 1982 Cyclic nucleotides and lipolysis in rat fat cells.
647 Interaction between calcium ionophore A23187 and FCCP, uncoupler
648 of oxidative phosphorylation. *Life Science* **32** 571–576.
649 Gaur S, Yamaguchi H & Goodman HM 1996a Growth hormone regulates
650 cytosolic free calcium in rat fat cells by maintaining L-type calcium
651 channels. *The American Journal of Physiology* **270** C1478-84.
652 Gaur S, Yamaguchi H & Goodman HM 1996b Growth hormone increases
653 calcium uptake in rat fat cells by a mechanism dependent on protein
654 kinase C. *American Journal of Physiology-Cell Physiology* **270** C1485–
655 C1492. (doi:10.1152/ajpcell.1996.270.5.c1485)
656 Gaur S, Schwartz Y, Tai LR, Frick GP & Goodman HM 1998 Insulin
657 produces a growth hormone-like increase in intracellular free calcium
658 concentration in okadaic acid-treated adipocytes. *Endocrinology* **139**
659 4953–4961. (doi:10.1210/endo.139.12.6387)

660 Gorzelniak K, Janke J, Engeli S & Sharma AM 2001 Validation of
661 endogenous controls for gene expression studies in human adipocytes
662 and preadipocytes. *Hormone and Metabolic Research* **33** 625–627.
663 (doi:10.1055/s-2001-17911)
664 El Hachmane MF & Olofsson CS 2018 A mechanically activated TRPC1-like
665 current in white adipocytes. *Biochemical and Biophysical Research*
666 *Communications* **498** 736–742. (doi:10.1016/j.bbrc.2018.03.050)
667 El Hachmane MF, Ermund A, Brännmark C & Olofsson CS 2018
668 Extracellular atp activates store-operated Ca2+ entry in white
669 adipocytes: functional evidence for STIM1 and ORAI1. *Biochemical*
670 *Journal* **475** 691–704. (doi:10.1042/BCJ20170484)
671 Hardy RW, Ladenson JH, Hruska KA, Jiwa AH & McDonald JM 1992 The
672 effects of extracellular calcium and epinephrine on cytosolic-free
673 calcium in single rat adipocytes. *Endocrinology* **130** 3694–3702.
674 (doi:10.1210/en.130.6.3694)
675 Hell JW, Buonarati OR, Henderson PB, Horne MC & Murphy GG 2017
676 Proteolytic processing of the L-type Ca2+ channel alpha 11.2 subunit
677 in neurons. *F1000Research* **6**. (doi:10.12688/f1000research.11808.1)
678 Henneman E & Mendell LM 2010 Functional Organization of Motoneuron
679 Pool and its Inputs. In *Comprehensive Physiology*. John Wiley & Sons,
680 Inc. (doi:10.1002/cphy.cp010211)
681 Hvarfner A, Bergström R, Lithell H, Mörlin C, Wide L & Ljunghall S 1988
682 Changes in calcium metabolic indices during long-term treatment of
683 patients with essential hypertension. *Clinical Science* **75** 543–549.
684 Izawa T, Koshimizu E, Komabayashi T & Tsuboi M 1983 Effects of Ca2+
685 and calmodulin inhibitors on lipolysis induced by epinephrine,
686 norepinephrine, caffeine and ACTH in rat epididymal adipose tissue.
687 *Nihon Seirigaku Zasshi. Journal of the Physiological Society of Japan*
688 **45** 36–44.
689 Kelly KL, Jude T & Corkey BE 1989 Cytosolic Free Calcium in Adipocytes.
690 *Biochemistry* 12754–12757.
691 Komai AM, Brännmark C, Musovic S & Olofsson CS 2014 PKA-independent

cAMP stimulation of white adipocyte exocytosis and adipokine secretion: modulations by Ca $^{2+}$ and ATP. *The Journal of Physiology* **592** 5169–5186. (doi:10.1113/jphysiol.2014.280388)

Lee SC & Pappone PA 1997 Membrane responses to extracellular ATP in rat isolated white adipocytes. *Pflugers Archiv European Journal of Physiology* **434** 422–428. (doi:10.1007/s004240050416)

Lipscombe D 2004 L-Type Calcium Channels: The Low Down. *Journal of Neurophysiology* **92** 2633–2641. (doi:10.1152/jn.00486.2004)

Louis C, Van Den Daelen C, Tinant G, Bourez S, Thomé JP, Donnay I, Larondelle Y & Debier C 2014 Efficient in vitro adipocyte model of long-term lipolysis: A tool to study the behavior of lipophilic compounds. *In Vitro Cellular and Developmental Biology - Animal* **50** 507–518. (doi:10.1007/s11626-014-9733-6)

Martin BBR, Clausen T & Gliemannt J 1975 Relationships between the Exchange of Calcium and Phosphate in Isolated Fat-Cells. *Biochemical Journal* **152** 121–129.

Miyauchi A, Hruska KA, Greenfield EM, Duncan R, Alvarez J, Barattolo R, Colucci S, Zambonin-Zallone A, Teitelbaum SL & Teti A 1990 Osteoclast cytosolic calcium, regulated by voltage-gated calcium channels and extracellular calcium, controls podosome assembly and bone resorption. *The Journal of Cell Biology* **111** 2543–2552. (doi:10.1083/JCB.111.6.2543)

N'Gouemo P, Akinfiresoye LR, Allard JS & Lovinger DM 2015 Alcohol withdrawal-induced seizure susceptibility is associated with an upregulation of CaV1.3 channels in the rat inferior colliculus. *International Journal of Neuropsychopharmacology* **18** 1–7. (doi:10.1093/ijnp/pyu123)

Ni Z, Smogorzewski M & Massry SG 1994 Effects of parathyroid hormone on cytosolic calcium of rat adipocytes. *Endocrinology* **135** 1837–1844. (doi:10.1210/en.135.5.1837)

Ni Z, Smogorzewski M & Massry SG 1995 Elevated cytosolic calcium of adipocytes in chronic renal failure. *Kidney International* **47** 1624–

724 1629. (doi:10.1038/ki.1995.226)
725 Pepe S, Bogdanov K, Hallaq H, Spurgeon H, Leaf A & Lakatta E 2006
726 Omega 3 polyunsaturated fatty acid modulates dihydropyridine effects
727 on L-type Ca2+ channels, cytosolic Ca2+, and contraction in adult rat
728 cardiac myocytes. *Proceedings of the National Academy of Sciences*
729 **91** 8832–8836. (doi:10.1073/pnas.91.19.8832)
730 Pershadsingh HA, Lee LY & Snowdowne KW 1989 Evidence for a
731 sodium/calcium exchanger and voltage-dependent calcium channels
732 in adipocytes. *FEBS Letters* **244** 89–92. (doi:10.1016/0014-
733 5793(89)81169-X)
734 Pfaffl MW 2001 A new mathematical model for relative quantification in
735 real-time RT-PCR. *Nucleic Acids Research* **29** 16–21.
736 (doi:10.1093/nar/29.9.e45)
737 Raifman TK, Kumar P, Haase H, Klussmann E, Dascal N & Weiss S 2017
738 Protein kinase C enhances plasma membrane expression of cardiac L-
739 type calcium channel, CaV1.2. *Channels* **11** 604–615.
740 (doi:10.1080/19336950.2017.1369636)
741 Ramírez-Ponce M, Acosta J & Bellido J 1990 Electrical activity in white
742 adipose tissue of rat. *Revista Espanola de Fisiologia* **46** 133–138.
743 Rueden CT, Schindelin J, Hiner MC, DeZonia BE, Walter AE, Arena ET &
744 Eliceiri KW 2017 ImageJ2: ImageJ for the next generation of scientific
745 image data. *BMC Bioinformatics* **18** 1–26. (doi:10.1186/s12859-017-
746 1934-z)
747 Rumiantsev D, Piotrovskii V, Metelitsa V, Slastnikova I, Martsevich Yu S &
748 Kokurina E 1989 Serum binding of nifedipine and verapamil in
749 patients with ischaemic heart disease on monotherapy. *British Journal*
750 *of Clinical Pharmacology* **28** 357–361. (doi:10.1111/j.1365-
751 2125.1989.tb05438.x)
752 Sattar N & Gill JM 2014 Type 2 diabetes as a disease of ectopic fat ? *BMC*
753 *Medicine* **12** 1–6. (doi:10.1186/s12916-014-0123-4)
754 Schimmel R 1978 Calcium Antagonists and Lipolysis in Isolated Rat
755 Epididymal Adipocytes: Effects of Tetracaine, Manganese, Cobaltous

and Lanthanum Ions and D600. *Hormone and Metabolic Research* **10** 128–134. (doi:10.1055/s-0028-1093458)

Schroeder A, Mueller O, Stocker S, Salowsky R, Leiber M, Gassmann M, Lightfoot S, Menzel W, Granzow M & Ragg T 2006 The RIN: an RNA integrity number for assigning integrity values to RNA measurements. *BMC Molecular Biology* **7** 3. (doi:10.1186/1471-2199-7-3)

Schulla V, Renström E, Feil R, Feil S, Franklin I, Gjinovci A, Jing X-J, Laux D, Lundquist I, Magnuson MA *et al.* 2003 Impaired insulin secretion and glucose tolerance in beta cell-selective Ca(v)1.2 Ca2+ channel null mice. *The EMBO Journal* **22** 3844–3854. (doi:10.1093/emboj/cdg389)

Schwartz Y, Goodman HM & Yamaguchi H 1991 Refractoriness to growth hormone is associated with increased intracellular calcium in rat adipocytes. *Proceedings of the National Academy of Sciences of the United States of America* **88** 6790–6794. (doi:10.1073/PNAS.88.15.6790)

Le Scouarnec S, Bhasin N, Vieyres C, Hund TJ, Cunha SR, Koval O, Marionneau C, Chen B, Wu Y, Demolombe S *et al.* 2008 Dysfunction in ankyrin-B-dependent ion channel and transporter targeting causes human sinus node disease. *Proceedings of the National Academy of Sciences of the United States of America* **105** 15617–15622. (doi:10.1073/pnas.0805500105)

Seydoux J, Muzzin P, Moinat M, Pralong W, Girardier L & Giacobino J-PP 1996 Adrenoceptor heterogeneity in human white adipocytes differentiated in culture as assessed by cytosolic free calcium measurements. *Cellular Signalling* **8** 117–122. (doi:10.1016/0898-6568(95)02035-7)

Shi L, Ko ML & Ko GY-P 2017 Retinoschisin Facilitates the Function of L-Type Voltage-Gated Calcium Channels. *Frontiers in Cellular Neuroscience* **11** 232. (doi:10.3389/fncel.2017.00232)

Silver N, Cotroneo E, Proctor G, Osailan S, Paterson KL & Carpenter GH 2008 Selection of housekeeping genes for gene expression studies in

the adult rat submandibular gland under normal, inflamed, atrophic and regenerative states. *BMC Molecular Biology* **9** 1–15. (doi:10.1186/1471-2199-9-64)

Soma MR, Gotto AM & Ghiselli G 1989 Rapid modulation of rat adipocyte lipoprotein lipase: effect of calcium, A23187 ionophore, and thrombin. *Biochimica et Biophysica Acta (BBA) - Lipids and Lipid Metabolism* **1003** 307–314. (doi:10.1016/0005-2760(89)90237-3)

Wang Z, Li V, Chan GCK, Phan T, Nudelman AS, Xia Z & Storm DR 2009 Adult type 3 adenylyl cyclase-deficient mice are obese. *PLoS ONE* **4** e6979. (doi:10.1371/journal.pone.0006979)

Xu W & Lipscombe D 2001 Neuronal Ca(V)1.3alpha(1) L-type channels activate at relatively hyperpolarized membrane potentials and are incompletely inhibited by dihydropyridines. *The Journal of Neuroscience : The Official Journal of the Society for Neuroscience* **21** 5944–5951. (doi:21/16/5944 [pii])

Yue F, Cheng Y, Breschi A, Vierstra J, Wu W, Ryba T, Sandstrom R, Ma Z, Davis C, Pope BD *et al.* 2014 A comparative encyclopedia of DNA elements in the mouse genome. *Nature* **515** 355–364. (doi:10.1038/nature13992)

Ziegler R, Jobst W, Minne H & Faulhaber JD 1980 Calciotropic hormones and lipolysis of human adipose tissue: role of extracellular calcium as conditioning but not regulating factor. *Endokrinologie* **75** 77–88.

812 **Table 1.** Primer sequences

Name	Accession number	Sequence	Product Size (bp)
Beta-actin	V01217	FWD: 5'-AGGCCCAGAGCAAGAGAG-3' REV: 5'-CCTCATAGATGGGCACAGT-3’	333
18s rRNA	V01270	FWD: 5'-TCTGCCCTATCAACTTTCGATG-3' REV: 5'-AATTTGCGCGCCTGCTGCCTTCCTT-3'	137
Cacna1s (CaV1.1)	U31816.1	FWD: 5'-CAAGTCCTTCCAGGCCCTG-3’ REV: 5'-CGTAGTCAGACTCCGGGTCG-3'	271
Cacna1c (CaV1.2)	M67515.1	FWD: 5'-CGCATTGTCAATGACACGATC-3' REV: 5'-CGGCAGAAAGAGCCCTTGT-3'	217
Cacna1d (CaV1.3)	M57682.1	FWD: 5'-TTGGTACGGACGGCTCTCA-3' REV: 5'-CCCCACGGTTACCTCATCAT-3’	156
Cacna1f (CaV1.4)	U31816.1	FWD: 5'- AGCACAAGACCGTAGTGGTG-3' REV: 5'- ATACCCCCAATGCCACACAG-3’	168
Cacnb1	NM_017346.1	FWD: 5’-AGTGCCAACAGAAGCAGAAGT-3’ REV: 5’-GTGTTTGCTGGGGTTGTTGAG-3’	237
Cacnb2	NM_053851.1	FWD: 5’-CTCTTCTTCCCCTGCACCAA-3’ REV: 5’-GCCTCGGCTAAGAGCAGTTT-3’	237
Cacnb3	NM_012828	FWD: 5’-CCTACGCCCGGGTTTGA-3’ REV: 5’-CAAATGCCACAGGTTTGTGCT-3’	174
Cacnb4	NM_001105733.1	FWD: 5’-ATGCCAGGTCTGCATGTCTC-3’ REV: 5’-ACATGGGGGTCTGGTGATCC-3’	231
Cacna2d1	NM_012919.3	FED: 5’-CCAAATCTCAGGAGCCGGT-3’ REV: 5’-GCAATACCAAGGCCAAACTGT-3’	219
Cacna2d2	NM_175592.2	FWD: 5’-CTGCAGGTCAAGTTGCCAAT -3’ REV: 5’-AGACGCGTTCCACTAACTGC -3’	262
Cacna2d3	NM_175595	FWD: 5’-TGGACGAGAGGCTGCTTTTG-3’ REV: 5’-ATGTACGCTTCGGTCCACAC-3’	180
Cacna2d4	NM_001191751.1	FWD: 5’-ATCGCCTTCGACTGCAGAAA-3’ REV: 5’-CTCTCGGTTGTCTCGATCCG-3’	255

813

814 **Table 2.** Primer sequences used for qPCR analysis

Name	Sequence	Product Size (bp)
Hprt1	FWD:5'- CGAGGAGTCCTGTTGATGTTGC -3' REV:5'- CTGGCCTATAGGCTCATAGTGC -3’	172
Pgk1	FWD:5'- TAGTGGCTGAGATGTGGCACAG -3' REV:5'- GCTCACTTCCTTTCTCAGGCAG -3'	166
GAPDH	FWD:5'- GGCAAGTTCAATGGCACAGT -3 REV:5'- TGGTGAAGACGCCAGTAGACTC -3'	183

815

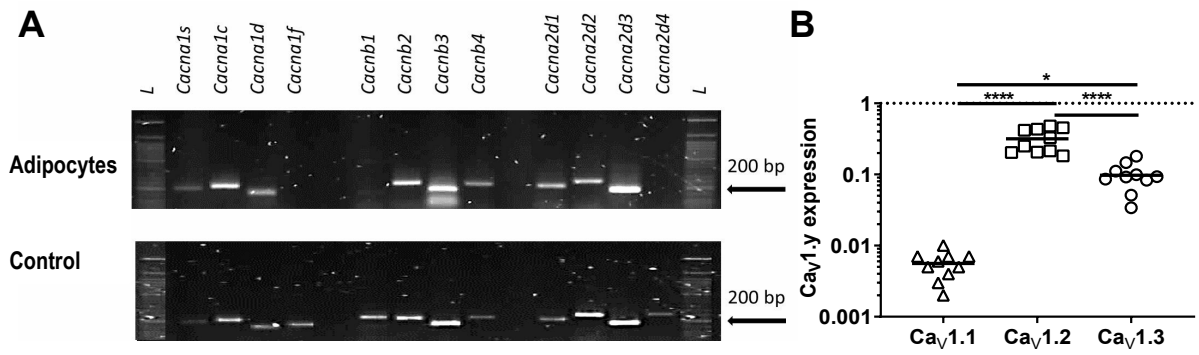

Figure 1. $Ca_V1.1$, 1.2 and 1.3 mRNA are expressed in rat adipocytes. A) RT-CPR products (Rattus norvegicus) of voltage-dependent L-type calcium channels $Ca_V1.1$, $Ca_V1.2$, $Ca_V1.3$ and $Ca_V1.4$ $alpha_1$ (*cacna1s, cacna1c, cacna1d* and *cacna1f*), $beta_2$ (*cacnb1, cacnb2, cacnb3* and *cacnb4*) and $alpha_2delta$ (*cacna2d1, cacna2d2, cacna2d3* and *cacna2d4*) subunits for white fat adipocytes and for control: skeletal muscle for *cacna1s* ($Ca_V1.1$) and whole brain for all other genes; L , DNA 50 bp ladder. PCR product sizes are in Table 1. B) Relative expression of $Ca_V1.1$, $Ca_V1.2$ and $Ca_V1.3$ alpha-1 subunits as determined by qPCR. Data is normalized to mRNA expression of $Ca_V1.2$ in rat brain. Each point represents a different animal (n=10), horizontal line is mean. Statistical significance is by one-way ANOVA, with Tukey's multiple comparison test.

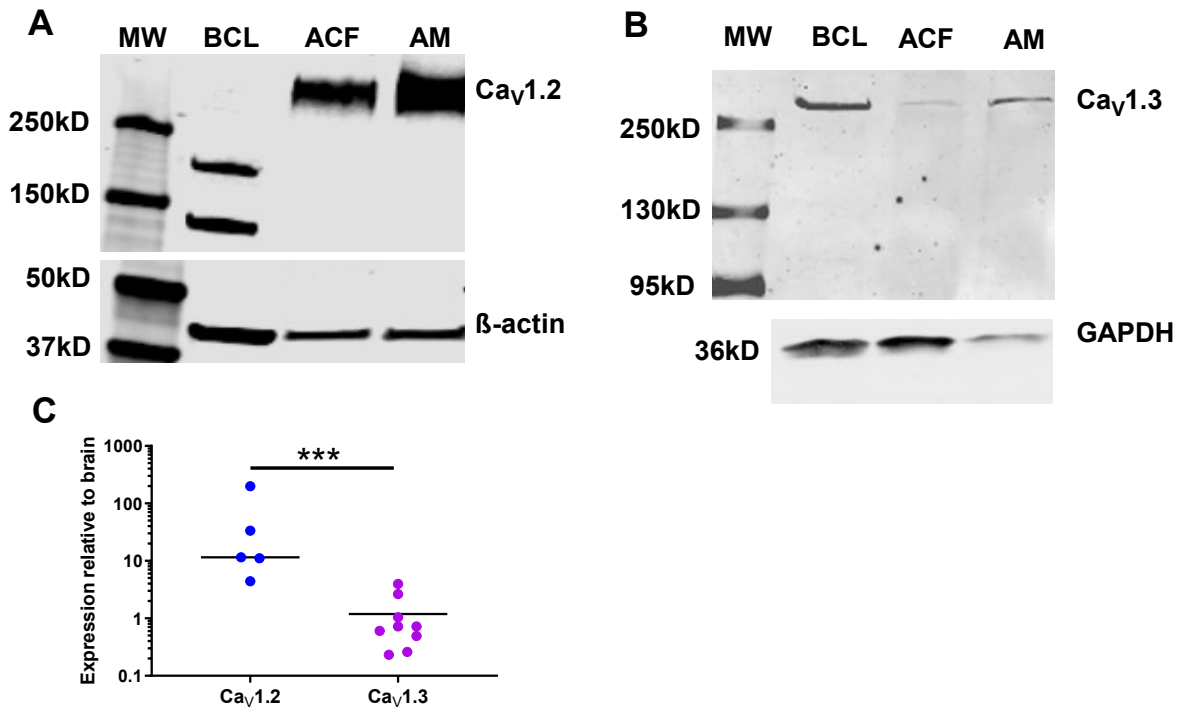

Figure 2. White fat adipocytes express $Ca_V1.2$ and $Ca_V1.3$ protein in membrane fractions. Representative Western blots of $Ca_V1.2$ (A) and $Ca_V1.3$ (B) in adipocyte cell lysate fraction (ACF) and membrane fraction (AM) of white fat adipocytes. Note the larger molecular weight (MW) of the $Ca_V1.2$ protein in adipocytes: >250 kD compared to the proteolytic cleavage product of 210 kD in the whole brain cell lysate (BCL) positive control. C) Relative protein expression of $Ca_V1.2$ (n=5) to $Ca_V1.3$ (n=9) in membrane fractions from white fat adipocytes. Data normalized to beta-actin. Horizontal lines are the medians. Statistical significance is by Mann Whitney.

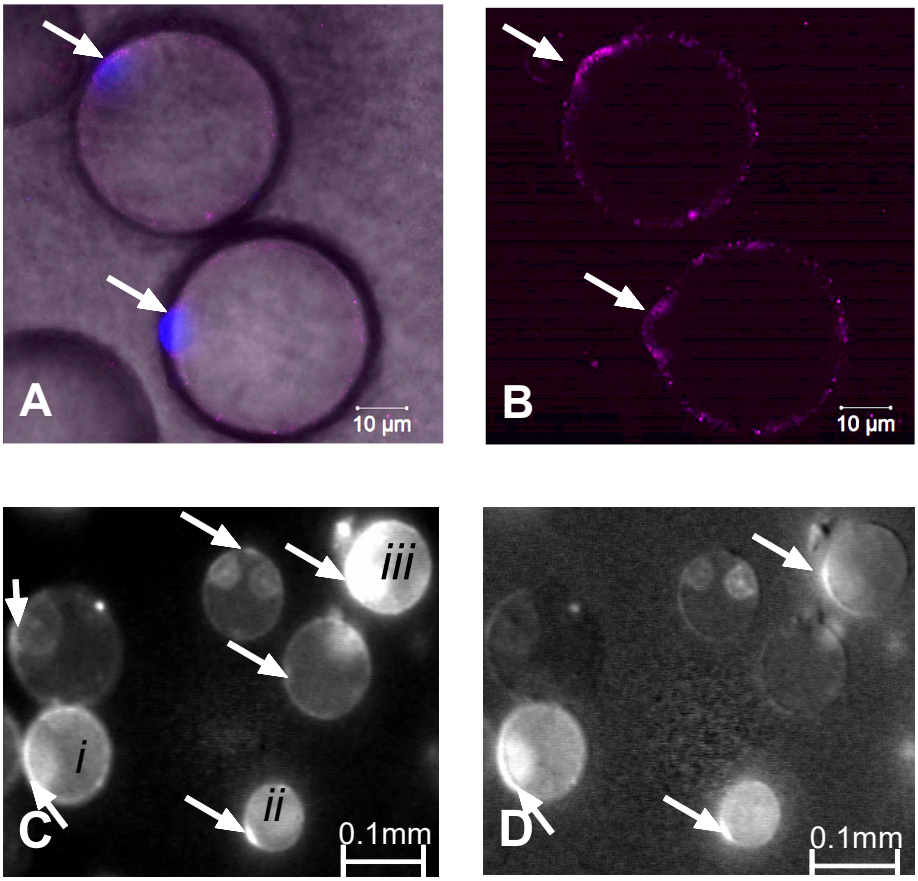

Figure 3. $Ca_V1.2$ in the plasma-membrane. A and B Confocal images of fixed rat epididymal white fat adipocytes. A) Blue, nucleus stained with Hoechst 33342; Magenta, Atto 594 labelled antibody to $Ca_V1.2$. Image captured over 62s. B) Magenta only channel to highlight $Ca_V1.2$ labelling which is densest in the nuclear region. Arrows indicate associated nuclei. C and D greyscale epifluorescent Ca^{2+} images of a field of 6 rat epididymal white fat adipocytes. C) Adipocytes under basal conditions, arrows indicate nuclei. Note nuclear protuberances and brighter circumferential fluorescence where the cytoplasm has the deepest volume parallel to the plane of illumination. D) Image shown in C is ratioed to that observed in the absence of extracellular Ca^{2+} to normalize dye loading and cytoplasmic volume. The brighter fluorescence in the perinuclear region of cells *i, ii,* and *iii* indicates a higher Ca^{2+} level. C and D are averages of 100 frames.

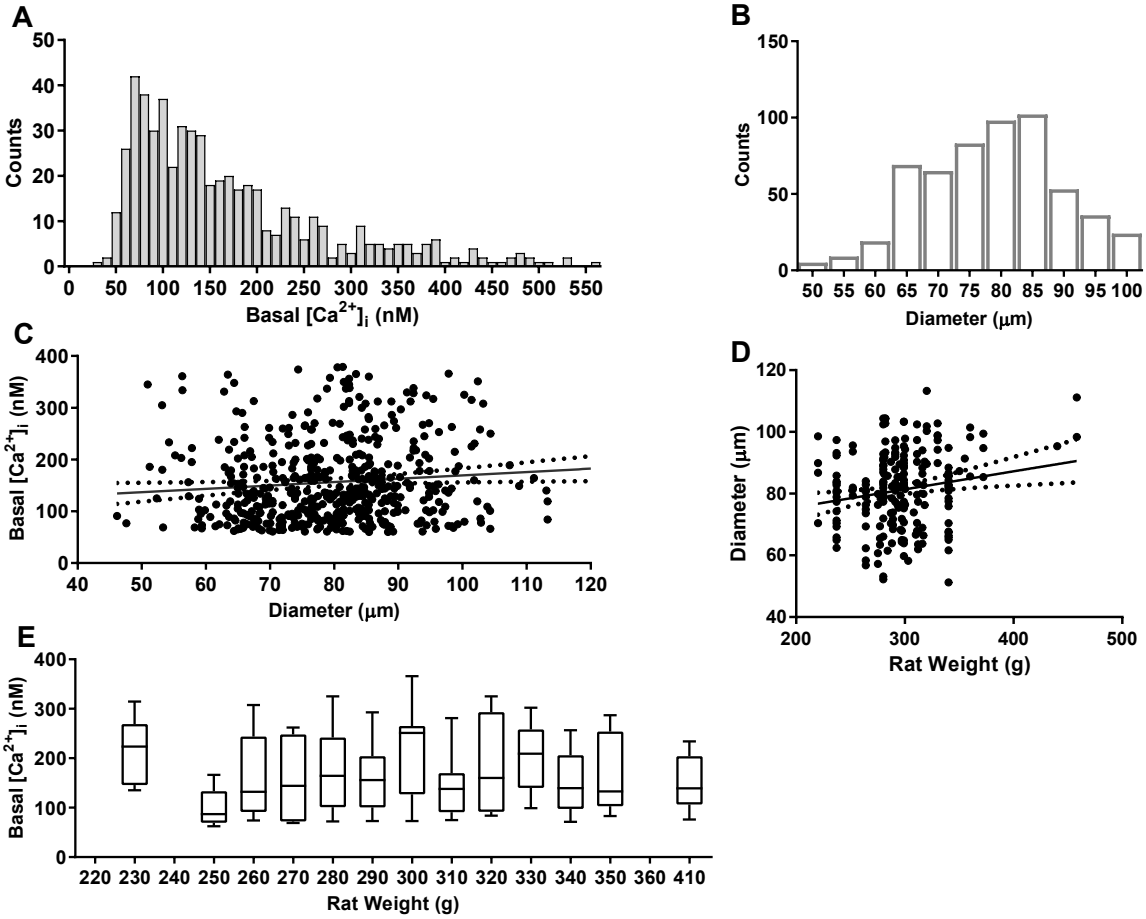

Figure 4. Measurement of intracellular $[Ca^{2+}]_i$ in isolated adipocytes

A) Distribution of basal $[Ca^{2+}]_i$ (n = 588). B) Distribution of adipocyte diameters (n = 547). C) Scatter plot of $[Ca^{2+}]_i$ versus cell diameter (n= 495). D) Scatter plot of cell diameter for 233 adipocytes with each vertical data set taken from a given weighed animal (45 in total). Solid lines in C) & D) are drawn by linear regression with slopes of 0.65 ± 0.29 nM μM^{-1} ($p< 0.03$) and 0.058 ± 0.02 μm g^{-1} ($p < 0.01$) respectively. Dotted lines are 95% C.I. for the fits shown. E) Individual distributions of basal $[Ca^{2+}]_i$ for epididymal adipocytes from 13 different rats (n = 7-40). Note the variation in $[Ca^{2+}]_i$ within any given animal was greater than between animals (ANOVA).

876

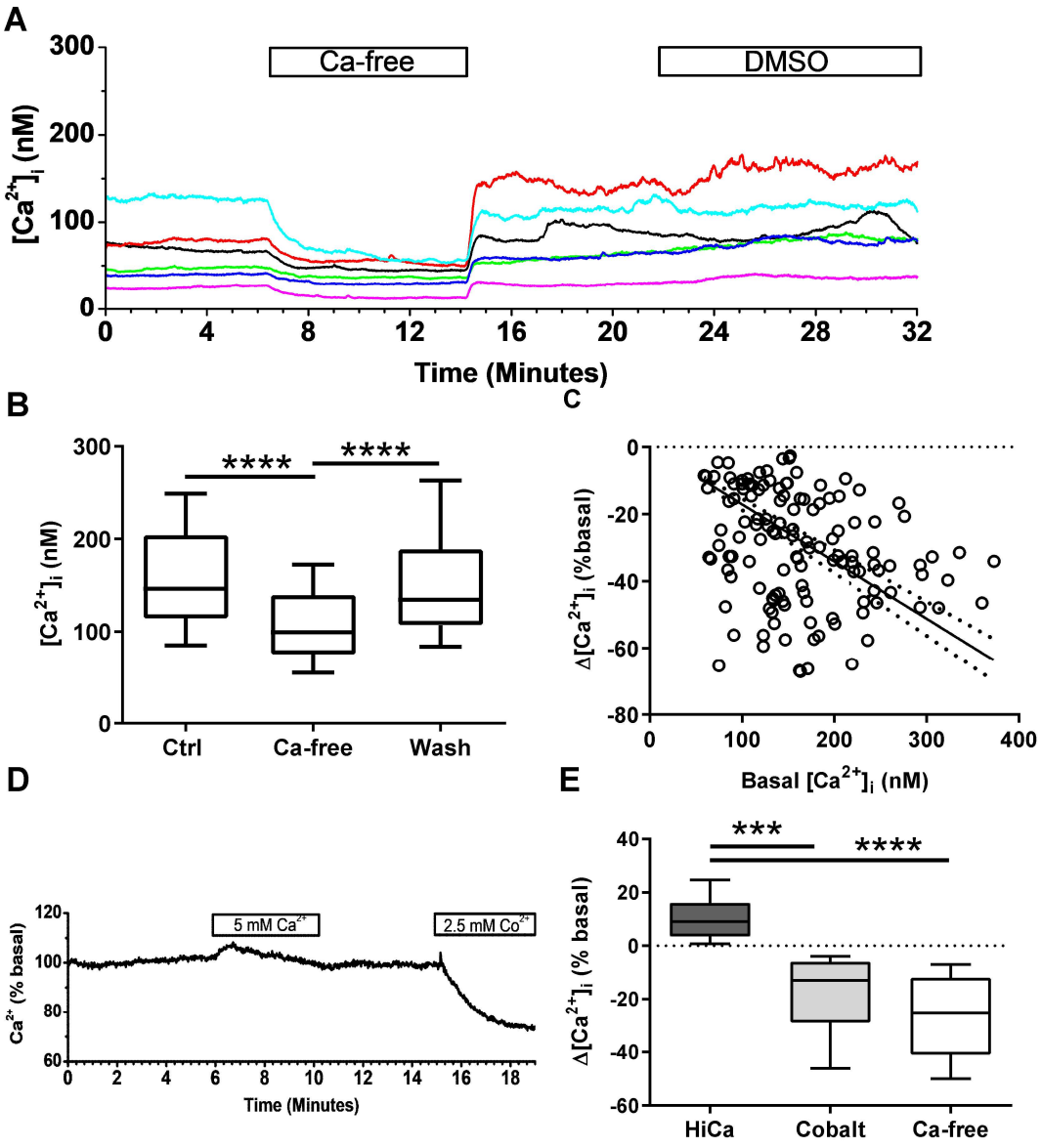

877

878 **Figure 5. Extracellular Ca^{2+} removal decreases intracellular**
879 **$[Ca^{2+}]_i$** A) $[Ca^{2+}]_i$ time courses measured for 6 adipocytes within a single
880 field in response to removal of bath Ca^{2+} (Ca-free), followed by 0.1%
881 DMSO. B) $[Ca^{2+}]_i$ in control (Ctrl), after removal of extracellular Ca^{2+} (Ca-
882 free) and recovery (Wash) (n = 138). Statistical inference by Friedman with
883 Dunn's multiple comparison tests. C) Relationship between the decrease
884 in $[Ca^{2+}]_i$, $\Delta[Ca^{2+}]_i$, on removal of bath $Ca^{2+}$and basal $[Ca^{2+}]_i$. Solid line
885 drawn by linear regression with a slope of -0.17 ± 0.01 % nM^{-1} ($p<$
886 0.0001). Dotted lines are the 95% C.I. for the fit shown. D) Mean time

887 course of $[Ca^{2+}]_i$ for 5 adipocytes in response to 5 mM $CaCl_2$ (HiCa) followed
888 by 2.5 mM $CoCl_2$ (Cobalt) added to the bath. E) $\Delta[Ca^{2+}]_i$ responses to HiCa
889 (n = 17), Cobalt (n = 19) and removal of extracellular Ca^{2+} (Ca-free; n =
890 140). Dashed line indicates no effect. Data is from 7 animals. Statistical
891 inference was by Kruskal-Wallis with Dunn's multiple comparison tests.
892

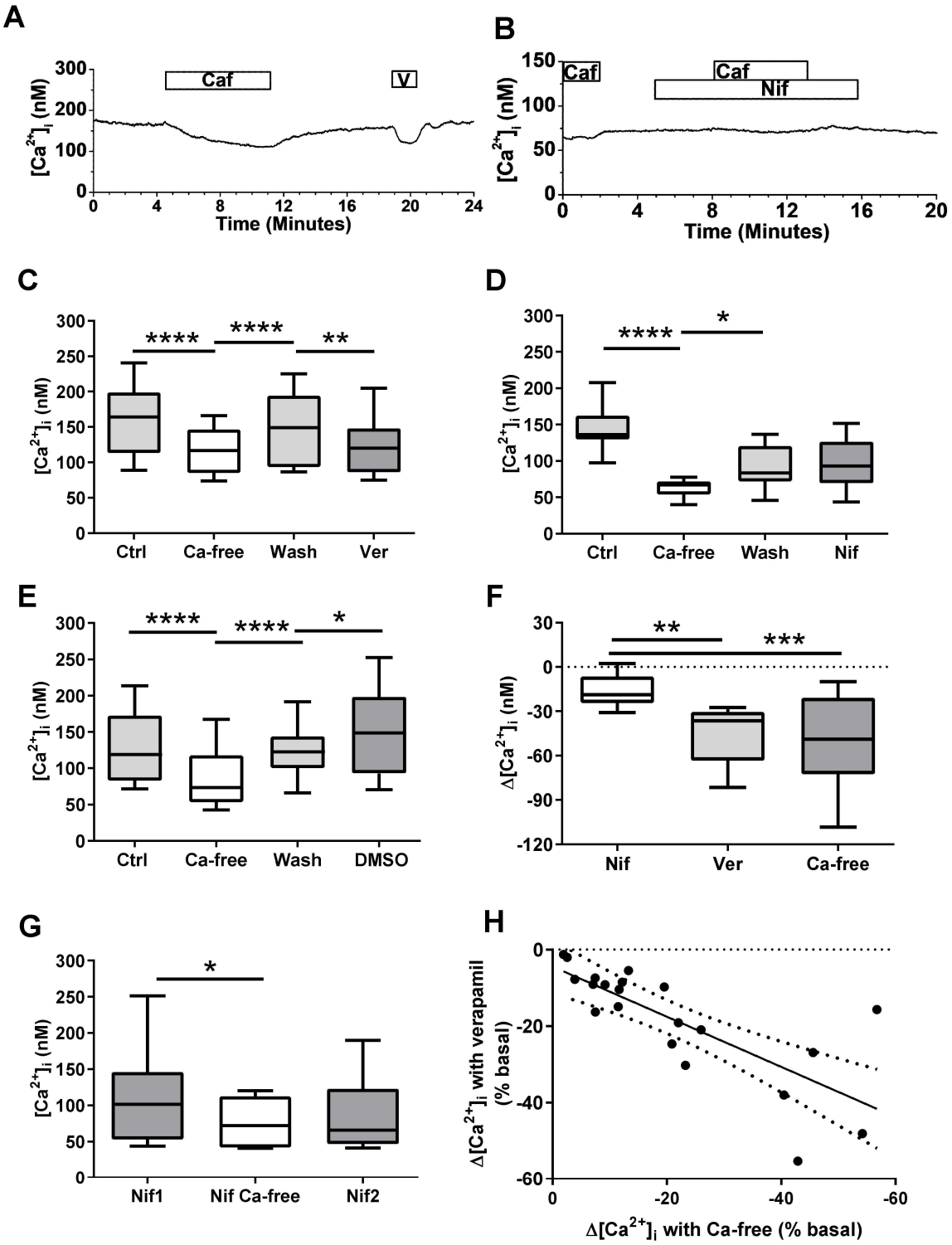

Figure 6. Verapamil and nifedipine decrease the intracellular Ca^{2+} concentration, $[Ca^{2+}]_I$ A) Mean time course of $[Ca^{2+}]_i$ measured for 11 adipocytes within a single field in response to removal of bath Ca^{2+} (Caf), followed by 20 μM verapamil (V). B) Mean time course of $[Ca^{2+}]_i$ measured for a field of 5 adipocytes in response to removal of bath Ca^{2+} (Cafr) in the

absence and then presence of 20 μM nifedipine (Nif). Note block by nifedipine is countered by a positive DMSO effect on fluorescence. C) $[Ca^{2+}]_i$ in control (Ctrl), after removal of extracellular Ca^{2+} (Ca-free) and recovery (Wash) followed by 20 μM verapamil (Ver) (n= 19 from 6 animals). D) $[Ca^{2+}]_i$ in control (Ctrl), after removal of extracellular Ca^{2+} (Ca-free) and recovery (Wash) followed by the addition of 20 μM nifedipine (Nif) (n = 15 from 4 animals). E) $[Ca^{2+}]_i$ in control (Ctrl), after removal of extracellular Ca^{2+} (Ca-free) and recovery (Wash) followed by 0.1% DMSO (n = 36 from 6 animals). F) Comparison of $\Delta[Ca^{2+}]_i$ produced by removal of bath Ca^{2+} (Ca-free), 20 μM nifedipine (Nif; n = 15) and 20 μM verapamil (Ver; n = 19). Data are from C and D and are corrected for DMSO effects shown in E (n = 137). G) $[Ca^{2+}]_i$ in the continuous presence of 20 μM nifedipine (Nif1) where Ca^{2+} is removed from the bath (Nif Ca-free) and added back again (Nif2) (n= 9 from 2 animals). For C-G, statistical comparison between groups was by Kruskal-Wallis with Dunn's multiple comparison tests. H) Relationship between $\Delta[Ca^{2+}]_i$ produced by 20 μM verapamil and removal of bath Ca^{2+} (n = 21) for the same cell. Solid line is linear regression of data with a slope of 0.66 ± 0.13. The dotted lines are the 95% C.I. of the fit.

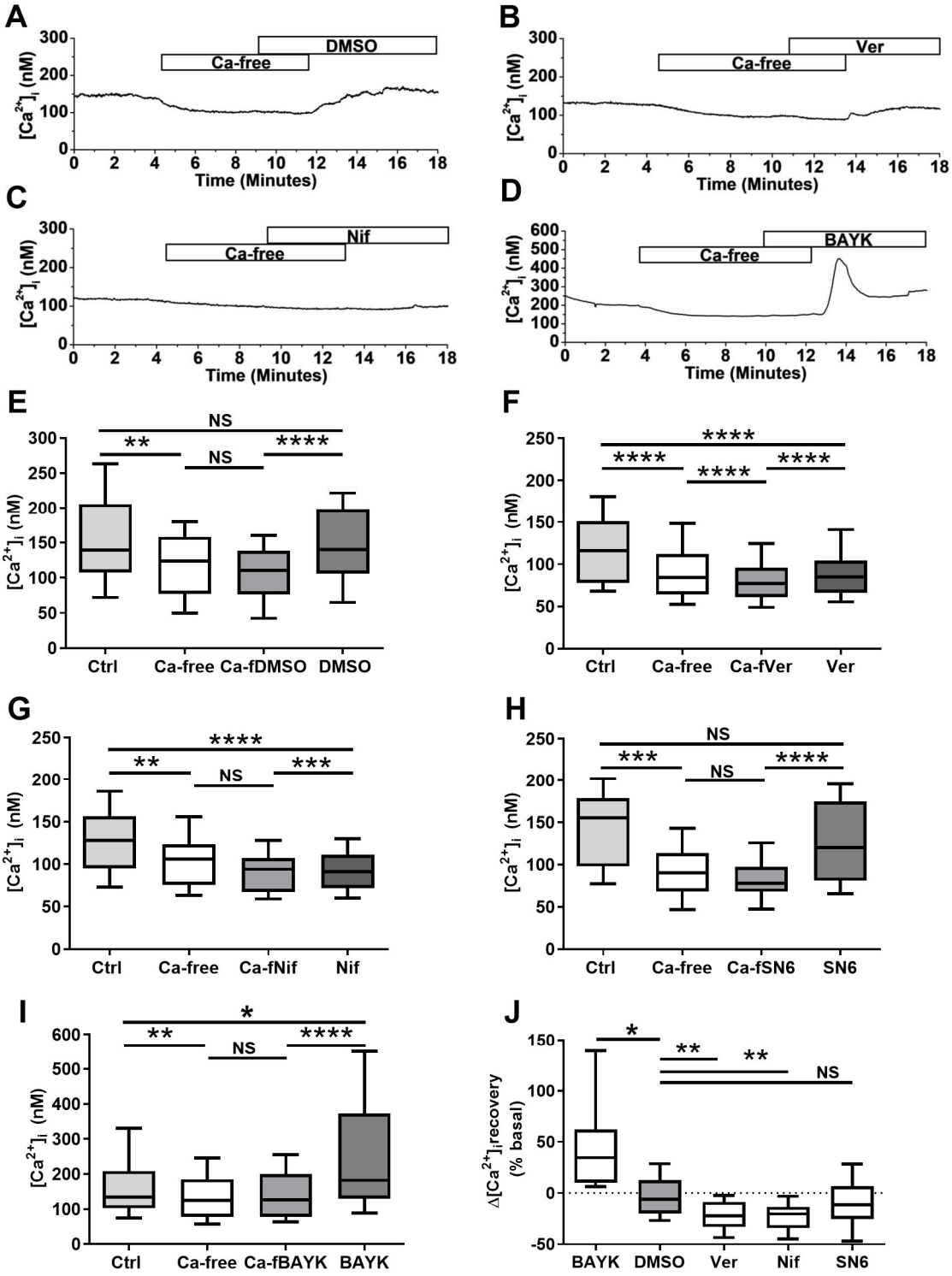

Figure 7. Pharmacological exploration of Ca^{2+} recovery. A-D) Representative mean time courses of $[Ca^{2+}]_i$ in response to removal of bath Ca^{2+} (Ca-free) followed by the addition of drugs as indicated.: A) 0.1% vovl/vol DMSO; B) 20 μM verapamil (V); C) 20 μM nifedipine (Nif); D) 10 μM BAY-K8644 (BAYK) all in Ca^{2+} free. E) $[Ca^{2+}]_i$ in control (Ctrl), after

removal of extracellular Ca^{2+} (Ca-free), after addition of 0.1% DMSO (Ca-fDMSO), then re-addition of bath Ca^{2+} in the presence of DMSO (DMSO) (n = 19 from 12 animals). F) $[Ca^{2+}]_i$ in control (Ctrl), after removal of extracellular Ca^{2+} (Ca-free), followed by 20 μM verapamil in Ca^{2+} free (Ca-fVer), then re-addition of bath Ca^{2+} in verapamil (Ver) (n = 67 from 12 animals). G) $[Ca^{2+}]_i$ in control (Ctrl), after removal of extracellular Ca^{2+} (Ca-free), followed by 20 μM nifedipine in Ca^{2+} free (Ca-fNif), then re-addition of bath Ca^{2+} in nifedipine (Nif) (n = 33 from 6 animals). H) $[Ca^{2+}]_i$ in control (Ctrl), after removal of extracellular Ca^{2+} (Ca-free), followed by 10 μM SN6 in Ca^{2+} free (Ca-fSN6), then re-addition of bath Ca^{2+} in SN6 (SN6) (n = 18 from 5 animals). I) $[Ca^{2+}]_i$ in control (Ctrl), after removal of extracellular Ca^{2+} (Ca-free), followed by 10 μM BAY-K8644 in Ca^{2+} free (Ca-fBAYK), then re-addition of bath Ca^{2+} in BAY-K8644 (BAYK) (n = 18 from 8 animals). All data uncorrected for DMSO effect. J) Percentage change in basal $[Ca^{2+}]_i$ after recovery on re-addition of bath Ca^{2+} with the various treatments as shown. Statistical comparison was by Friedman with Dunn's multiple comparison multiple comparison.

.

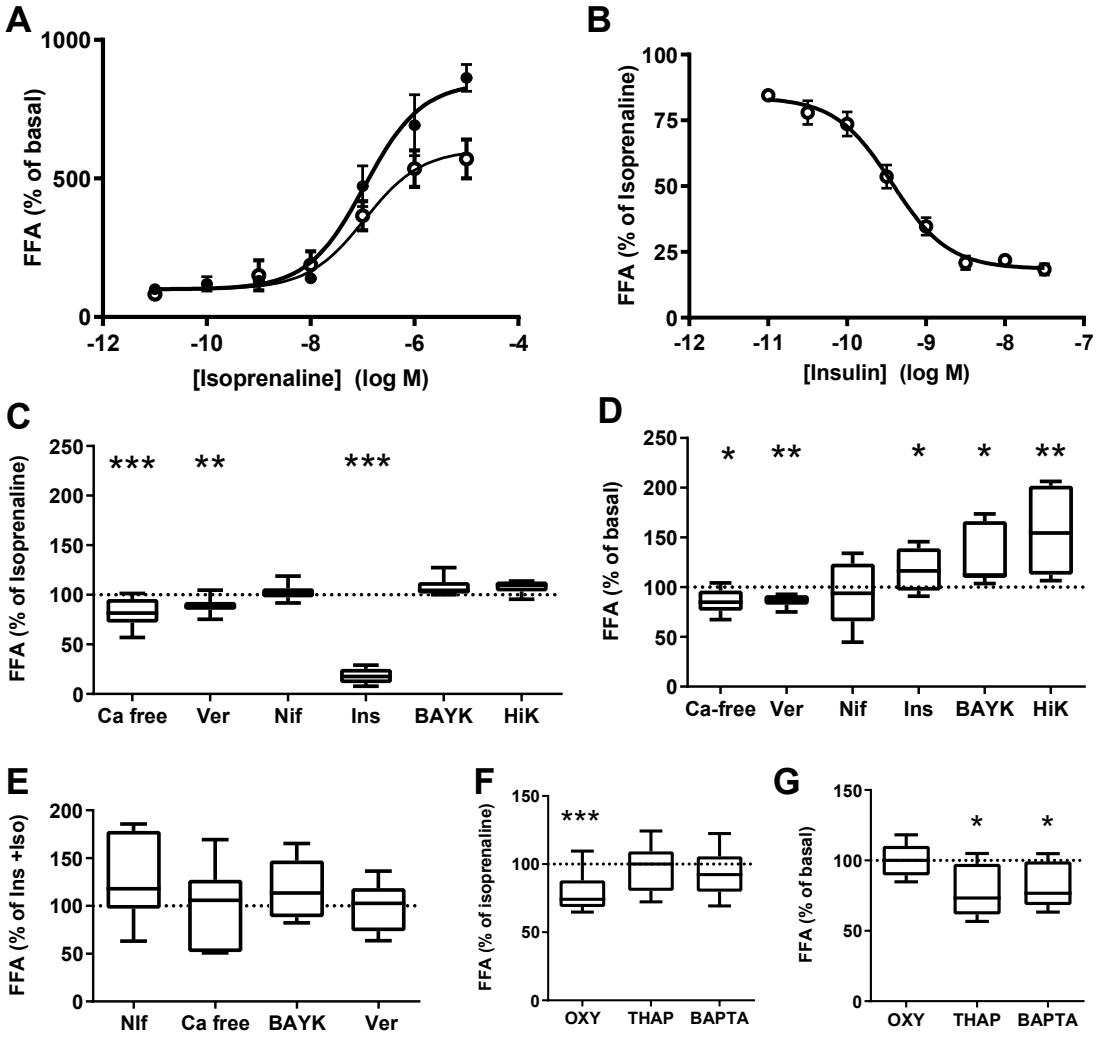

949

950 **Figure 8. Extracellular Ca^{2+}-influx potentiates lipolysis.** A) Lipolysis
951 as a function of isoprenaline in the presence (●) and absence (○) of bath
952 Ca^{2+}. Solid lines are fits of the data with sigmoidal dose response curves
953 with parameters given in the text. Data means ± S.E.M (n = 4-5). B)
954 Inhibition of lipolysis by insulin. Solid line is a fit of the data to dose-
955 response curve with parameters given in the text. Data are means ± S.E.M
956 (n = 5-9). C) Effects of interventions on lipolysis stimulated by 10 μM
957 isoprenaline: Ca free, removal of bath Ca^{2+}; Ver, 5 μM verapamil; Nif, 20
958 μM nifedipine; Ins, 20 nM insulin; BAYK, 1 μM BAY-K8644; HiK, 50 mM
959 bath $[K^+]_o$ (n = 6–16). D) Effects of interventions on basal lipolysis. Key as
960 for C (n = 6–16). E) Effects of interventions on beta-adrenoceptor mediated
961 lipolysis inhibited by 20 nM insulin: Key as for C (n = 6–10). F) Effects of
962 interventions on 10 μM isoprenaline stimulated lipolysis: OXY, 1 μM

963 oxytocin; THAP, 10 μM thapsigargin; BAPTA, 10 μM BAPTA-AM (n = 9–21).
964 G) Effects of interventions as shown in F on basal lipolysis. (n = 6–10).
965 DMSO the solvent for verapamil, nifedipine, and BAY-K8644 was without
966 effect on lipolysis. Statistics are Wilcoxon Sign test relative to 100%.
967
968

969

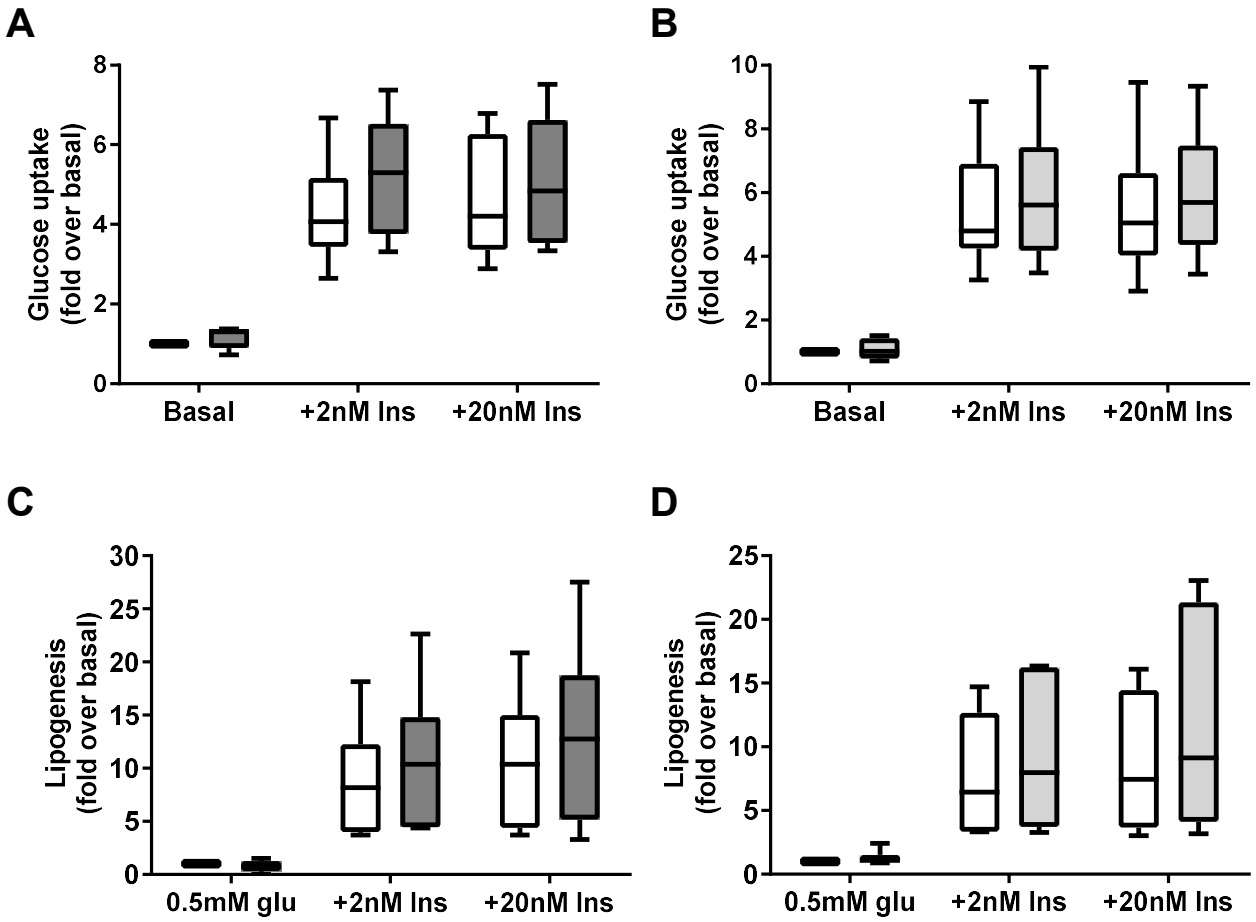

970

971 **Figure 9. Ca^{2+}-influx via L–Type VGCC does not affect glucose**
972 **uptake and lipogenesis.** A) Effect of 5 μM nifedipine on glucose uptake.
973 B) Effect of 1 μM BAY-K 8644 on glucose uptake. C) Effect of 5 μM nifedipine
974 on lipogenesis. D) Effect of 1 μM BAY-K 8644 on lipogenesis. Drug additions
975 are indicated by filled bars, controls by open bars, conditions are as
976 indicated. Ins, insulin, glu, glucose. Data are all paired with n=5 for each
977 condition. Statistical inference by Friedman's test.

978

979